The FEBS Journal

FEBS PRESS science publishing by scientists

Binding of different hyaluronan to CD44 mediates distinct cell adhesion dynamics under shear flow

Linda Li[1,2], Qihan Ding[1,3], Yi Wu[1,3], Zhi Zheng[1,3], Xiaoning Zhang[1,3], Mingkun Zhang[1,3], Mian Long[1,3] and Shouqin Lü[1,3]

1 Center of Biomechanics and Bioengineering, Key Laboratory of Microgravity (National Microgravity Laboratory), Beijing Key Laboratory of Engineered Construction and Mechanobiology, and CAS Center for Excellence in Complex System Mechanics, Institute of Mechanics, Chinese Academy of Sciences, Beijing, China

2 Key Laboratory of Biorheology Science and Technology, Ministry of Education, College of Bioengineering, Chongqing University, China

3 School of Engineering Science, University of Chinese Academy of Sciences, Beijing, China

Keywords

CD44; HA; molecular weight; shear flow; two-dimensional interaction

Correspondence

S. Lü and M. Long, Institute of Mechanics, Chinese Academy of Sciences, Beijing 100190, China

Tel: 86-10-82543778

E-mail: lsq@imech.ac.cn; mlong@imech.ac.cn

Linda Li and Qihan Ding contributed equally to this work.

(Received 28 January 2023, revised 30 April 2023, accepted 30 May 2023)

doi:10.1111/febs.16882

As a known receptor–ligand pair for mediating cell–cell or cell–extracellular matrix adhesions, cluster of differentiation 44 (CD44)-hyaluronan (HA) interactions are not only determined by molecular weight (MW) diversity of HA, but also are regulated by external physical or mechanical factors. However, the coupling effects of HA MW and shear flow are still unclear. Here, we compared the differences between high molecular weight HA (HHA) and low molecular weight HA (LHA) binding to CD44 under varied shear stresses. The results demonstrated that HHA dominated the binding phase but LHA was in favour of the shear resistance phase, respectively, under shear stress range ≤ 1.0 dyne·cm^{-2}. This difference was attributed to the high binding strength of the CD44–HHA interaction, as well as the optimal distribution matching between both CD44 and HA sides. Activation of the intracellular signal pathway was sensitive to both HA MW and shear flow. Our findings also indicate that only CD44–HHA interaction under shear stress of 0.2 dyne·cm^{-2} could significantly enhance the clustering of CD44, as well as induce the increase in both CD44 and CD18 expression. The present study offers the basis for further quantification of the features of CD44–HA interactions and their biological functions.

Introduction

Hyaluronan (HA) and cluster of differentiation 44 (CD44) are first recognized as a specific receptor–ligand pair for mediating cell adhesion between lymphoid and stromal cells [1], and further confirmed by a series of studies including T cell activation by HA bound CD44 [2], CD44–HA binding mediated lymphocyte cell rolling on endothelial under physiologic flow [3,4] and *in vivo* T cell extravasation into an inflamed site [5,6]. The functions of this counterparts are also extended to mediate neutrophil [7] and glioblastoma [8] cell adhesion and migration, as well as leukocyte adhesion in atherosclerotic initiation [9]. Specially, CD44–HA interactions [10,11], but not selectin-ligand interactions [12–14], dominate neutrophil sequestration in tissue specific liver sinusoids upon lipopolysaccharide stimulation. Evidently, CD44–HA interactions play key roles in mediating adhesion or migration of immune cells, stem cells or tumour cells. Thus

Abbreviations

2D, two-dimensional; AFM, atomic force microscopy; CD44, cluster of differentiation 44; DPBS, Dulbecco's phosphate-buffered saline; FITC, fluorescein isothiocyanate; HA, hyaluronan; HHA, high molecular weight HA; LFA-1, lymphocyte function-associated antigen 1; LHA, low molecular weight HA; MβCD, methyl-β-cyclodextrin; MW, molecular weight.

quantification of CD44–HA interactions is basic for understanding their biological functions.

First, CD44–HA interactions are more complicated than other receptor–ligand interactions because of the complexity of both CD44 and HA themselves. A typical feature is the diversity of HA molecular weight (MW) and distinct biological activities [15–18]. The composition and form of HA are defined by the balance of its synthesis and degradation. HA synthesis is performed by at least three distinct synthases (Has1–3), whereas the HA so formed can be fragmented by hyaluronidases, reactive oxygen or nitrogen species, resulting in a distinct MW. Generally, high molecular weight HA (HHA, commonly ≥ 1000 kDa) exist in almost all of the tissues under homeostatic conditions and function in suppressing inflammation, resulting in protective or healing effects to injury. However, low molecular weight HA (LHA, commonly 10–250 kDa) fragmentations are increased under pathological conditions, functioning in pro-inflammation with promoting disease progression [19]. The functional differences of HA MW are also reflected on CD44–HA interaction [20]. As demonstrated using single molecular level technologies of both atomic force microscopy (AFM) and friction force microscopy, the increase in HA MW enhances CD44–HA interactions and maximum binding occurs at ~1000 kDa HA, which is consistent with the MW dependence of cellular viability of CD44-positive cells that adhered on HA-coated substrate [21]. Similar results for the CD44–HA interaction are also obtained by surface plasma resonance with the increased binding affinity from LHA (6.4 kDa) to HHA (1500 kDa) resulting from the faster association and the slower dissociation for HHA. It is interesting that the CD44–HA interactions measured at cellular level show contrary results. CD44–LHA interaction mediates the strong single cell adhesion, consistent with the cellular function that immobilized LHA (30–50 kDa), but not HHA (500–750 kDa), in collagen matrices could enhance tumour cell invasion [22]. CD44–HHA interaction with HA immobilized in a layer-by-layer manner mediates the low cell adhesion and high cell motility of human gastric cancer cell line MKN45 [23]. These data confirmed that different HA MW have distinct binding abilities to CD44, and they can also induce distinct cellular functions. Unfortunately, the intrinsic relationship between CD44–HA interaction and biological function is still controversial. Furthermore, besides the HA MW difference in the above studies, versatile surface presentation characteristics of both HA and CD44, including different combinations of substrate/tip-anchored [21], soluble [24], collagen matrix-immobilized [22] or PLL-immobilized HA [23], and substrate-anchored [21,24] or cellular surface-expressed [21–24] CD44, highlight the difficulty with respect to direct comparisons of existing data.

In addition, compared with three-dimensional interactions where at least one partner of receptor or ligand exists in solution and has three-dimensional freedom, CD44–HA interactions for mediating cell–cell or cell-substrate adhesions belong to two-dimensional (2D) interactions because both of them are anchored to cellular surface or substrate respectively. This anchoring would confine their diffusion only along corresponding plane of anchoring [25,26]. The 2D feature renders that the CD44–HA interactions are not only determined by CD44 and HA themselves, but also regulated by external physical environments. For example, leukocyte adhesions mediated by CD44–HA interaction are involved in *in vivo* blood flow, and the shear stress suffered by adhered leukocytes under a blood flow environment would translate into an external force exerted onto the CD44–HA complex and further regulation of their dissociation. The transporting dynamics of leukocytes before adhesion in blood flow also affects the association of CD44–HA interaction and resulted cell adhesion. Indeed, a series of studies report the regulations of shear flow on CD44–HA interaction mediated adhesion. The adhesion number and rolling dynamics of $CD44^+$ cells by binding to HA coated substrate are sensitive to shear stress [27]. Different cell types expressing CD44 bound to the same HA-coated substrate show distinct adhesion resistances to shear stress [27,28]. However, the effect of HA MW on the sensitivity of CD44–HA interaction and how this further mediates cell adhesion to shear flow are still unclear.

Therefore, the coupling effects between HA MW and shear stress on CD44–HA interactions were tested in the present study. Using a flow chamber assay for mimicking *in vivo* blood flow, the regulations of distinct HA MW on CD44–HA interactions were quantified under shear flow through the index of cell adhesion dynamics. Their respective abilities with respect to inducing intracellular signal pathway were also explored. This work deepens our understanding of the contribution of CD44–HA interaction to the cell adhesion dynamics in the immunology response or tumour metastasis.

Results

HHA and LHA dominated distinct interactions to CD44 under shear flow

To test the effect of HA MW on CD44–HA interactions and corresponding biological function under

shear flow, a flow chamber assay was used to quantify their capabilities using U937 cell line expressing CD44 stably (data not shown). The specificity of CD44–HA interactions was first confirmed by results showing that both HHA (Fig. 1A,B) and LHA (Fig. 1C,D) could mediate effective adhesions of U937 under a shear flow of 0.2 dyne·cm^{-2}, but those control cases without HA coating or Hermes-1 blocking significantly reduced the adhered U937 number in the 300-s binding (Fig. 1A, C) and shear resistance phases (Fig. 1B,D). Next, the dependences of CD44–HHA/LHA interactions on shear flow demonstrated an interesting behaviour in that they were sensitive to shear flow and presented a threshold. Under low shear stresses of 0.1 and 0.2 dyne·cm^{-2}, the number of adhered cells mediated by CD44–HHA interaction increased gradually over time in the 300-s binding course from the higher initial number of around 50–60 cells, but almost kept constant under the higher shear flow of 0.5 and 1.0 dyne·cm^{-2} with the lower initial number of around 20 cells (Fig. 1E). This dependence of shear stress in the binding phase also affected the following shear resistance phase with distinct evolution profiles of adhered cell number between higher and lower shear stresses (Fig. 1F). The results mediated by CD44–LHA interactions showed a similar tendency (Fig. 1G, H), indicating that CD44–HA interactions were sensitive to shear stress with a threshold between 0.2 and 0.5 dyne·cm^{-2}. The association of CD44–HA interactions was dominant over the dissociation, resulting in a gradual increase in adhered cells below the threshold, but the association and dissociation reached a balance with almost constant adhered cells beyond the threshold.

CD44 binding differences between HHA and LHA were further compared under typical shear stresses of 0.2 and 0.5 dyne·cm^{-2}. The results showed that CD44–HHA interactions had a faster association with a quicker increase in adhered cell number from almost identical initial value of ~40 cells under a shear stress of 0.2 dyne·cm^{-2} (Fig. 2A) and yielded a similar pattern under 0.5 dyne·cm^{-2} with an even higher adhered cell number (Fig. 2C). By contrast, CD44–LHA interactions could resist shear stress more effectively with a slower decrease of adhered cell number in the shear resistance phase (Fig. 2B,D). The respectively dominant roles of HHA in the fast association and LHA in the ability to resist shear stress were not affected by the HA concentrations (2, 20, 200 or 1000 μg·mL^{-1}) used for substrate coating, even the differences between HHA and LHA were not always significant (data not shown). Thus, CD44–HHA interactions played dominant roles in the binding phase but CD44–LHA interactions were favourable for shear resistance under shear flow.

HHA and LHA presented distinct binding strengths to CD44

To explore the explanation for the differences between HHA and LHA binding to CD44 under shear flow, we first excluded the potential effect of HA coating number density. Noting that the HHA MW used here was about 50 times greater than the LHA MW (~1000 vs. ~20 kDa) and the above comparisons between HHA and LHA were based on the same HA mass concentration for substrate coating, one possible mechanism leading to the above differences may result from a lower HHA coating number density on the substrate as a result of its high MW compared to that of LHA, further affecting the binding ability to CD44. Here, we applied differential HHA and LHA with respective mass concentrations of 1000 and 20 μg·mL^{-1} in a flow chamber test, implying that this similar molar concentration could result in a comparable coating number density with the hypothesis of comparable coating efficiency. The results indicated that the dominated role of HHA in the binding phase disappeared (Fig. 2E,G), but that of LHA in shear resistance still existed at the end time point under 0.5 dyne·cm^{-2} (Fig. 2F,H). It was taken for granted that this matching of HA molar concentration for substrate coating would increase the coating number of HHA and reduce that of LHA compared to those shown in Fig. 2A–D with the same mass concentration of 200 μg·mL^{-1}. However, the vanishing difference between HHA and LHA in the binding phase and the intact difference in the shear resistance phase indicated that coating number density was not a deterministic factor for their difference.

We further measured the mechanical strength of CD44–HA interactions directly at the molecular level using an AFM assay to investigate their contributions to the differences between HHA and LHA. Specific bindings of CD44–HHA/LHA systems were represented by their significantly higher adhesion frequency compared to that of the control case under a contact duration of 500 ms (Fig. 3A–C). In addition, the systemic spring constant k, defined as the spring constant of the CD44–HA system in series with that of cantilever, was different between HHA and LHA. The CD44–LHA system had a higher k than that of the CD44–HHA system (Fig. 3D–F), which is reasonable because the CD44–LHA complex serves as a shorter spring than the CD44–HHA complex. A combination of these adhesion frequency and systemic spring constant tests validated the reliability of the AFM assay

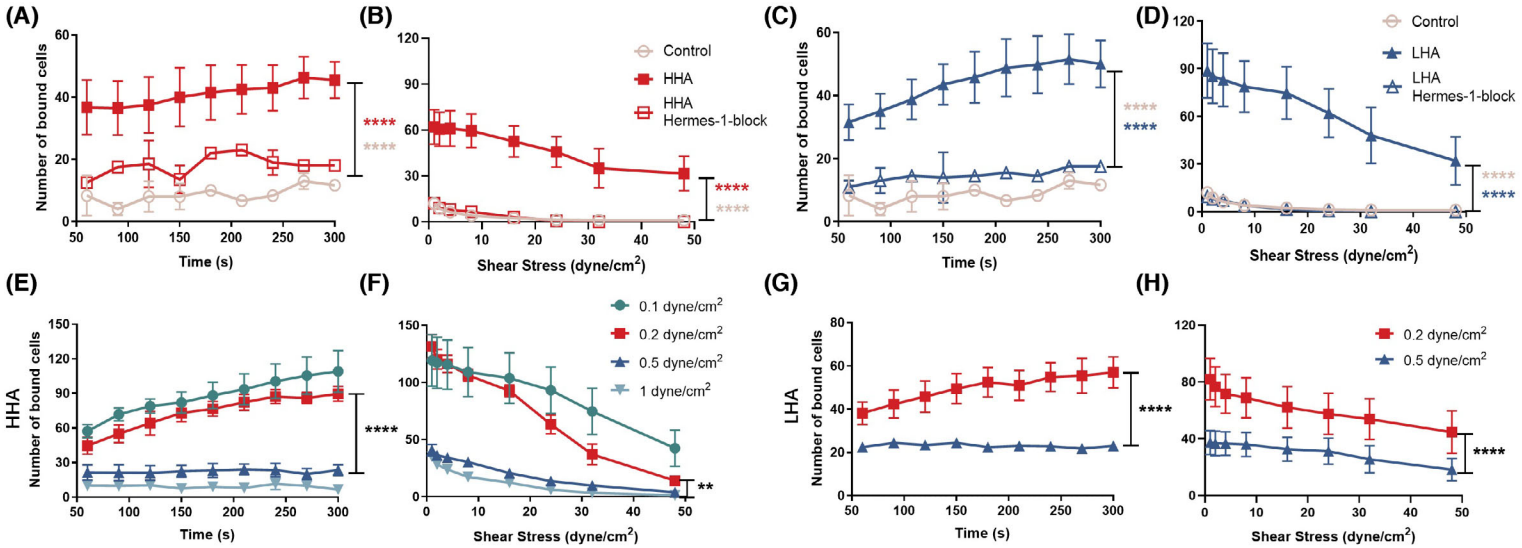

Fig. 1. Specificity of CD44–HA interaction and dependence of CD44–HA interaction-mediated cell adhesion on shear stress. (A–D) Specificity of CD44 binding to high molecular weight HA (HHA) (A, B) or low molecular weight HA (LHA) (C, D) interactions presented with respect to significant differences in the numbers of firmly adhered U937 cells in both binding (A, C) and shear resistance phases (B, D) compared to those in control case with blank substrate or blocking case by anti-CD44 blocking antibody Hermes-1. Shear stress in the binding phase was set as 0.2 dyne·cm^{-2}. (E–H) Evolution of number of firmly adhered cells under different shear stresses for both binding (E, G) and shear resistance (F, H) phases, respectively, mediated by CD44–HHA (E, F) and -LHA (G, H) interactions. The HA concentration for substrate coating was 1000 μg·mL^{-1}. Data are shown as the mean ± SE of at least three independent repeats. $^{**}P < 0.01$, $^{****}P < 0.0001$.

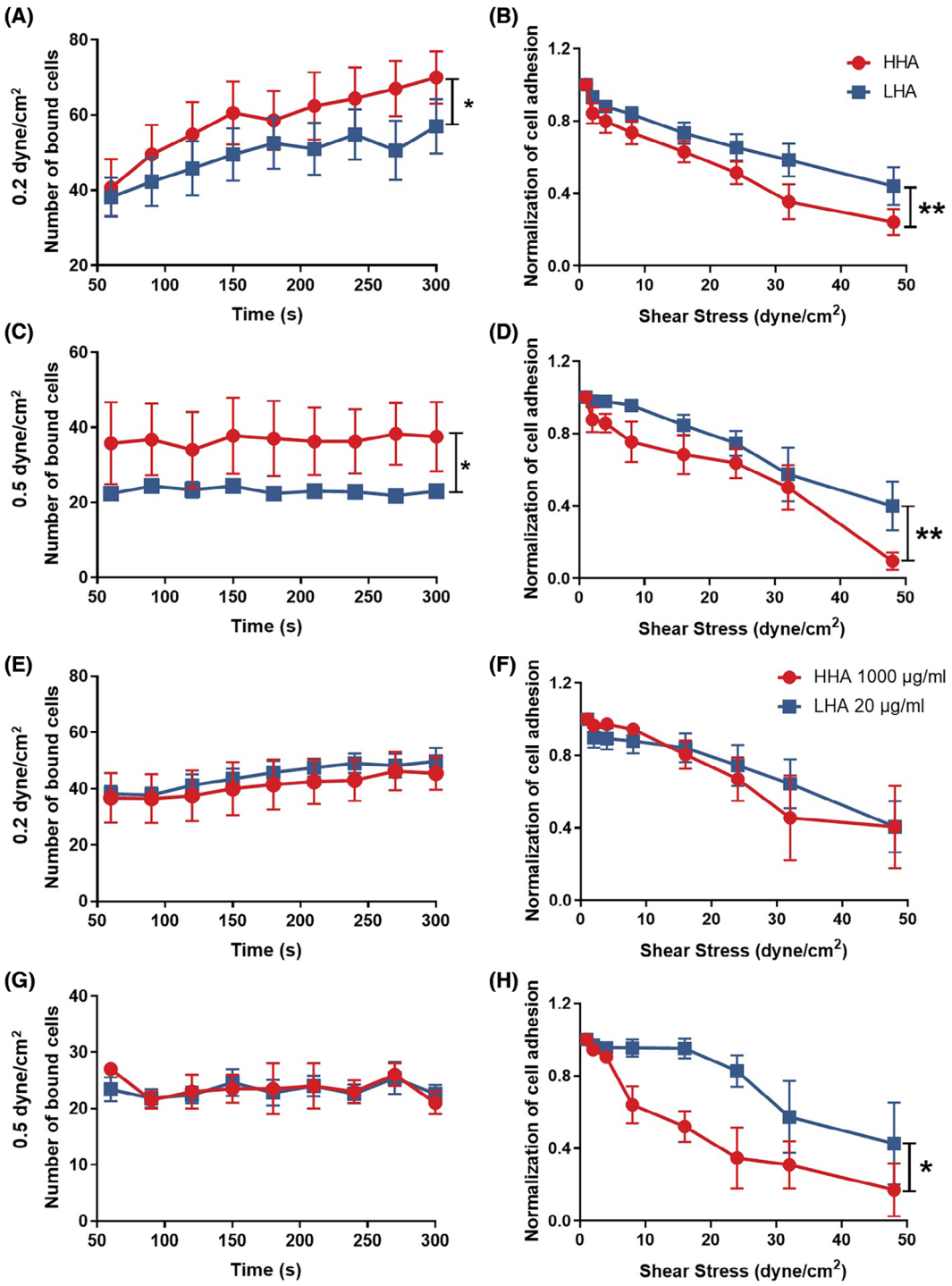

Fig. 2. Effects of HA molecular weight or concentration for substrate coating on HA-CD44 binding-mediated cell adhesion dynamics under shear flow. (A–D) Number of firmly adhered U937 cells in the binding phase (A, C) and evolutions of normalized firmly adhered cells in the shear resistance phase (B, D) mediated by CD44–HHA or -LHA interactions under shear stresses of 0.2 (A, B) and 0.5 (C, D) dyne·cm^{-2}, respectively. The concentration of HHA or LHA for substrate coating was 200 μg·mL^{-1}. (E–H) Comparisons of number of firmly adhered U937 cells in the binding phase (E, G) and evolution of normalized firmly adhered cells in the shear resistance phase (F, H) under shear stresses of 0.2 (E, F) and 0.5 (G, H) dyne·cm^{-2} between the HHA concentration of 1000 μg·mL^{-1} and LHA concentration of 20 μg·mL^{-1} coated substrates. Data are shown as the mean ± SE of at least three independent repeats. *$P < 0.05$, **$P < 0.01$.

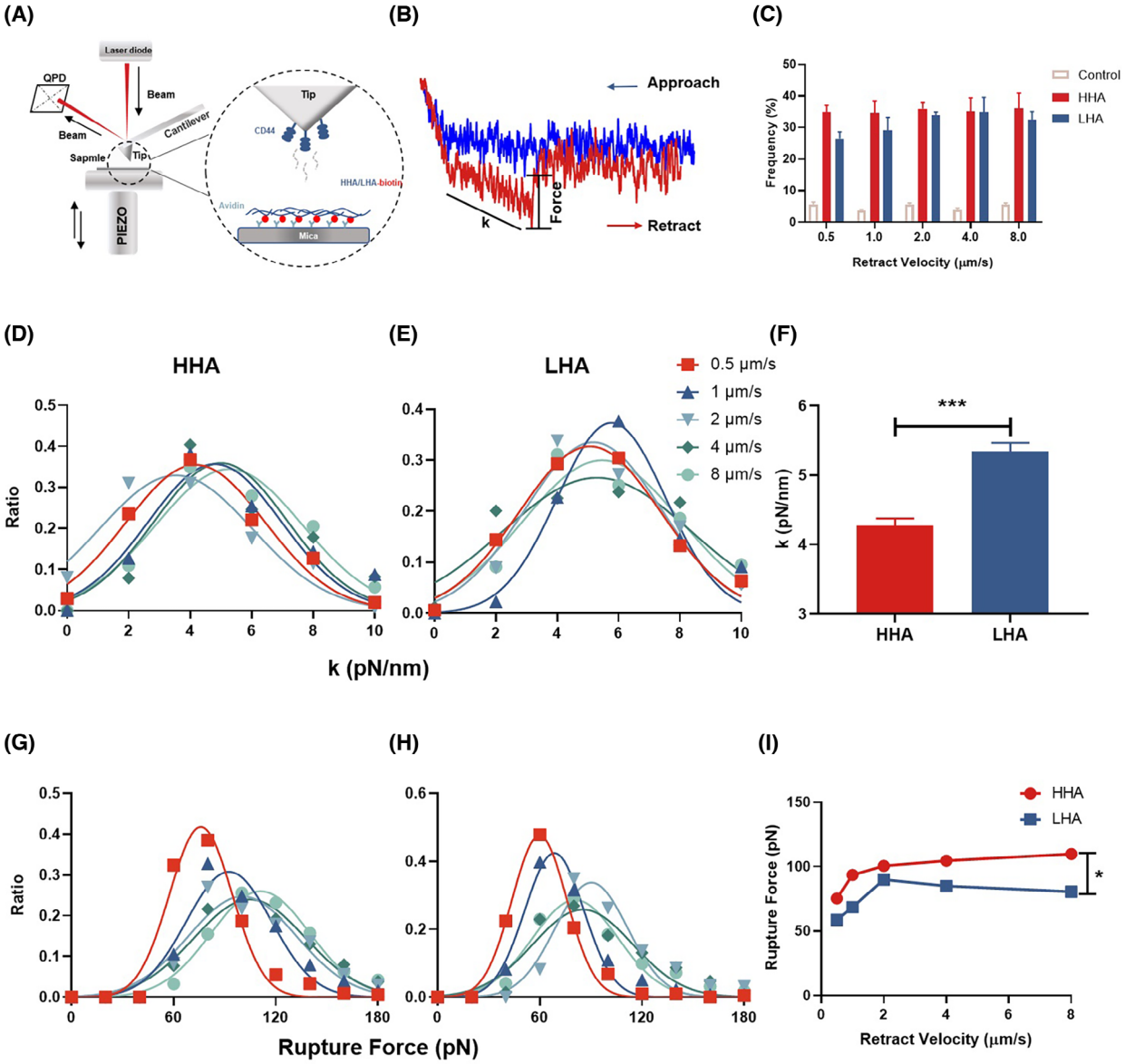

Fig. 3. Comparisons of spring constant and rupture force between HHA-CD44 and LHA-CD44 interactions by the AFM assay. (A) Schematic of AFM experimental set-up. The AFM cantilever was functionalized with CD44s by direct physical absorption. HHA/LHA-biotin was coated on substrate via avidin, respectively. Only avidin-adsorbed substrate served as a control. (B) Representative force curve of a complete cycle under force ramp mode. Blue and red traces were recorded for the approach and retraction of the cantilever, respectively. System spring constant k and rupture force F were measured for each force curve. (C) Adhesion frequencies under different retraction velocities. Spring constant (D, E) and rupture force (G, H) distributions of CD44–HHA (D, G) and CD44–LHA (E, H) complexes upon different retract velocities are shown with Gaussian fitting (lines) for each distribution. Averages of Gaussian fitting medians of all retract velocities for spring constant k and rupture force F are presented in (F) and (I), respectively. HA concentration was 200 μg·mL^{-1}. Approach velocity, contact force and contact time were 1 μm·s^{-1}, 150 pN and 500 ms, respectively, for all measurements. Data are shown as the mean ± SE of at least three independent experiments. *$P < 0.05$, ***$P < 0.001$.

for the measurement of CD44–HA interactions. Moreover, rupture force tests demonstrated that the CD44–HHA system presented higher rupture forces under various retract velocities (Fig. 3G–I). The higher mechanical strength for CD44–HHA interaction may partially explain its faster association and the quicker increase in adhered cell number observed in the binding phase of flow chamber assay.

CD44 distribution regulated HHA and LHA differences under shear flow

CD44 mainly expresses in the lipid raft on cell membrane [29,30], implying that CD44 distribution could be uneven in discrete clusters and the confinement of the lipid raft also reduces their diffusion along the cell membrane. This may in turn affect their binding to HA, such that the membrane distribution change of CD44 regulated by methyl-β-cyclodextrin (MβCD) modulates HA binding ability of CD44 in T lymphocytes and controls rolling dynamics under shear flow [29]. To quantify the effect of CD44 distribution pattern on its binding difference between HHA and LHA, we compared CD44–HA interactions before and after lipid raft disruption by MβCD. First of all, we confirmed that MβCD did not change the expression quantity of CD44 (Fig. 4A) but only caused the homogenization of distribution from local clustering (Fig. 4B). Flow chamber tests revealed that even expression of CD44 after MβCD treatment would enhance the shear resistance of CD44–HHA interaction but did not affect the binding dynamics much (Fig. 4C,D). However, the CD44–LHA interaction showed distinct effects with reduced binding dynamics but unchanged shear resistance after MβCD treatment (Fig. 4E,F). These differential effects indicated that the differences between HHA and LHA increased in the binding phase but disappeared for the shear resistance phase (Fig. 4G,H).

Indeed, the distribution of HHA coated on substrate in flow chamber assay could be regarded as a discrete LHA cluster, although that of LHA was relatively even under the same HA mass concentration. In combination with the above effects of CD44 distribution pattern on CD44–HA interactions, clustering of both or one side of receptor–ligand interaction pair was in favour of their association, although the uniform distribution of at least one side was beneficial to shear resistance. This was reasonable because local clustering would enhance the matching opportunity once they could reach each other. However, the shear resistance was affected by already bound molecular bonds, and a relatively even distribution of bonds could disperse the external force more effectively. These results also confirm the sensitivity of the 2D receptor–ligand interaction to external factors.

HHA and LHA induced distinct intracellular signals under shear flow

Besides initiating cell adhesion and implementing molecular recognition, CD44–HA interactions are also involved in rich intracellular signals endowed by the special location of CD44 in the lipid raft. For example, exogenous or constitutively expressed native HAs induce CD44 clustering [31] and CD44-anchored spectrins modulate the surface density of HA and sense and translate flow shear into changes in plasma membrane tension [32]. To evaluate the effect of HA MW on triggering intracellular signals, CD44 distribution and expression by binding to HHA or LHA were first compared. The results showed that CD44–HHA interaction could significantly enhance both CD44 clustering and expression under shear stress of 0.2 dyne·cm^{-2} compared to that of CD44–LHA interaction or a control case with blank substrate (Fig. 5A,B). The difference between HHA and LHA with respect to inducing CD44 clustering or expression disappeared under shear stress of 0.5 dyne·cm^{-2} or under static conditions (Fig. 5C,D).

Ligand binding to CD44 also can induce the activation of another cell adhesion molecule family of integrins. As a typical example, E-selectin binding to CD44 expressed on neutrophil membrane could induce the activation of lymphocyte function-associated antigen 1 (LFA-1) for neutrophil slow rolling in an inflammatory cascade [33]. Indeed, HA also has a similar ability, with CD44-engagement by HA binding enhancing the activation of very late antigen 4 [34] and CD44 cross-linking by 6.9 kDa LHA inducing the expression of LFA-1 on cancer cells [35]. Based on the above findings, we further investigated the abilities of HA MW with respect to activating integrin with a typical indicator of the CD18 integrin subfamily, known to express constitutively on leukocytes and to play key roles in mediating cell recruitment in immunoreaction by binding to their ligands. Interestingly, CD18 expression showed a similar tendency to that of CD44, as expected, and was also higher for the case of CD44–HHA interaction under shear stress of 0.2 dyne·cm^{-2} compared to other cases (Fig. 6). These results also confirmed that the sensitivities of CD44 and CD18 expression to HA MW and shear stress exposure depended on the existence of the lipid raft because the differences in their expression disappeared in the case of MβCD treatment regardless of HA MW and shear stress (Fig. 7). The above difference between HHA and LHA under shear stress of 0.2 dyne·cm^{-2} was also consistent with a spreading area of adhered cells (Fig. 8A). Accordingly, CD44–HHA interactions mediated the larger cell spreading area under 0.2 dyne·cm^{-2} compared to other cases, and the difference disappeared with MβCD treatment (Fig. 8B). In addition, the sensitivity of HA MW with respect to inducing CD44 and CD18 expression only relied on the

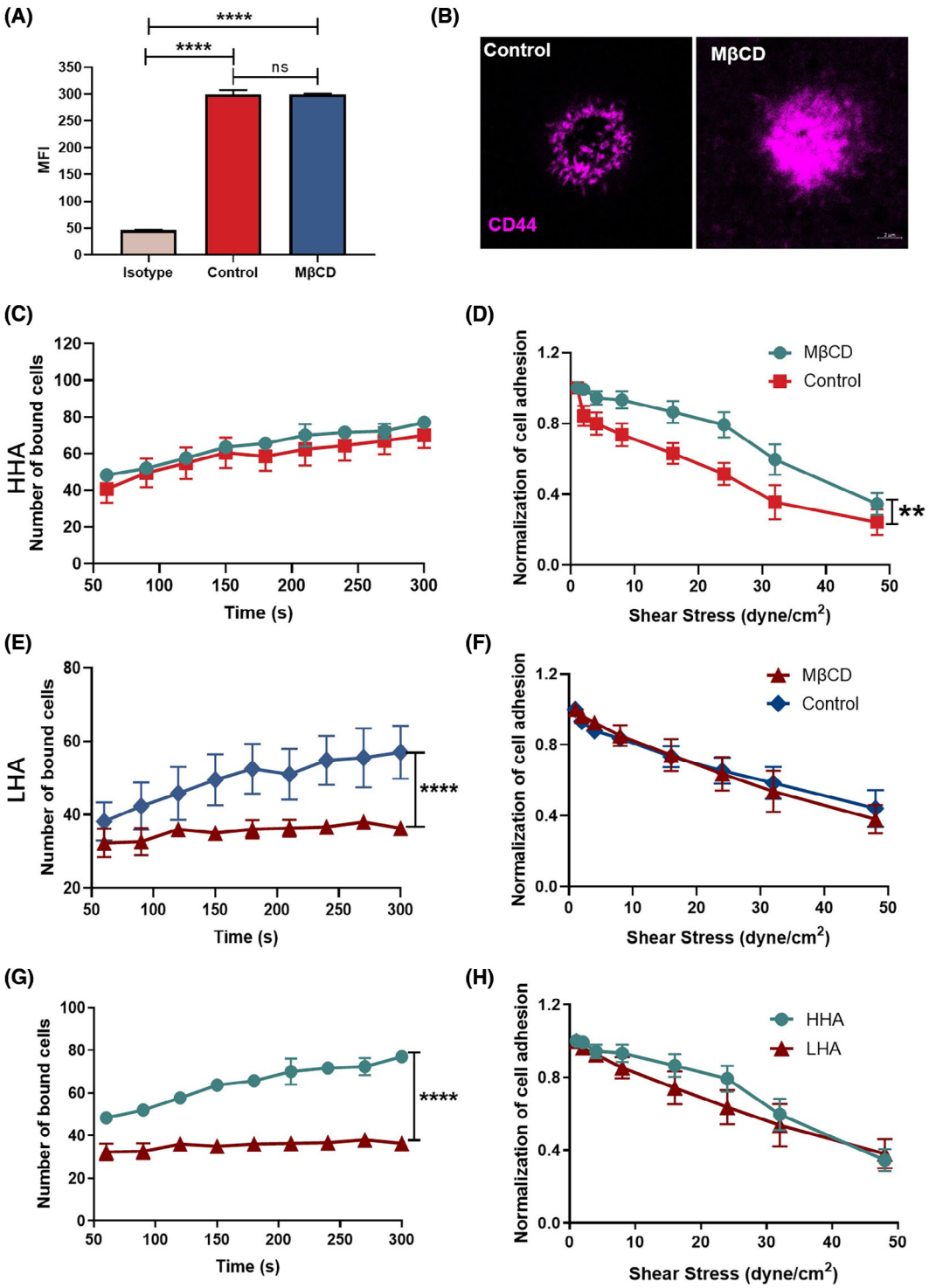

Fig. 4. Differences of cell adhesion dynamics induced by distinct CD44 distributions. Expression (A) and distribution pattern (B) of CD44 on U937 cells pre- or post-MβCD treatment were respectively quantified using flow cytometry or visualized using confocal microscopy. Scale bar = 2 μm (B). Comparisons of number of firmly adhered cells in the binding phase and evolution of normalized firmly adhered cells in shear resistance phase pre- and post-MβCD treatment are presented in (C, D) for CD44–HHA and (E, F) for CD44–LHA interactions. Corresponding comparisons between CD44–HHA and CD44–LHA interactions after MβCD treatment are shown in (G, H). Shear stress in the binding phase was 0.2 dyne·cm^{-2}. Data are shown as the mean ± SE of at least three independent repeats. $^{**}P < 0.01$, $^{****}P < 0.0001$.

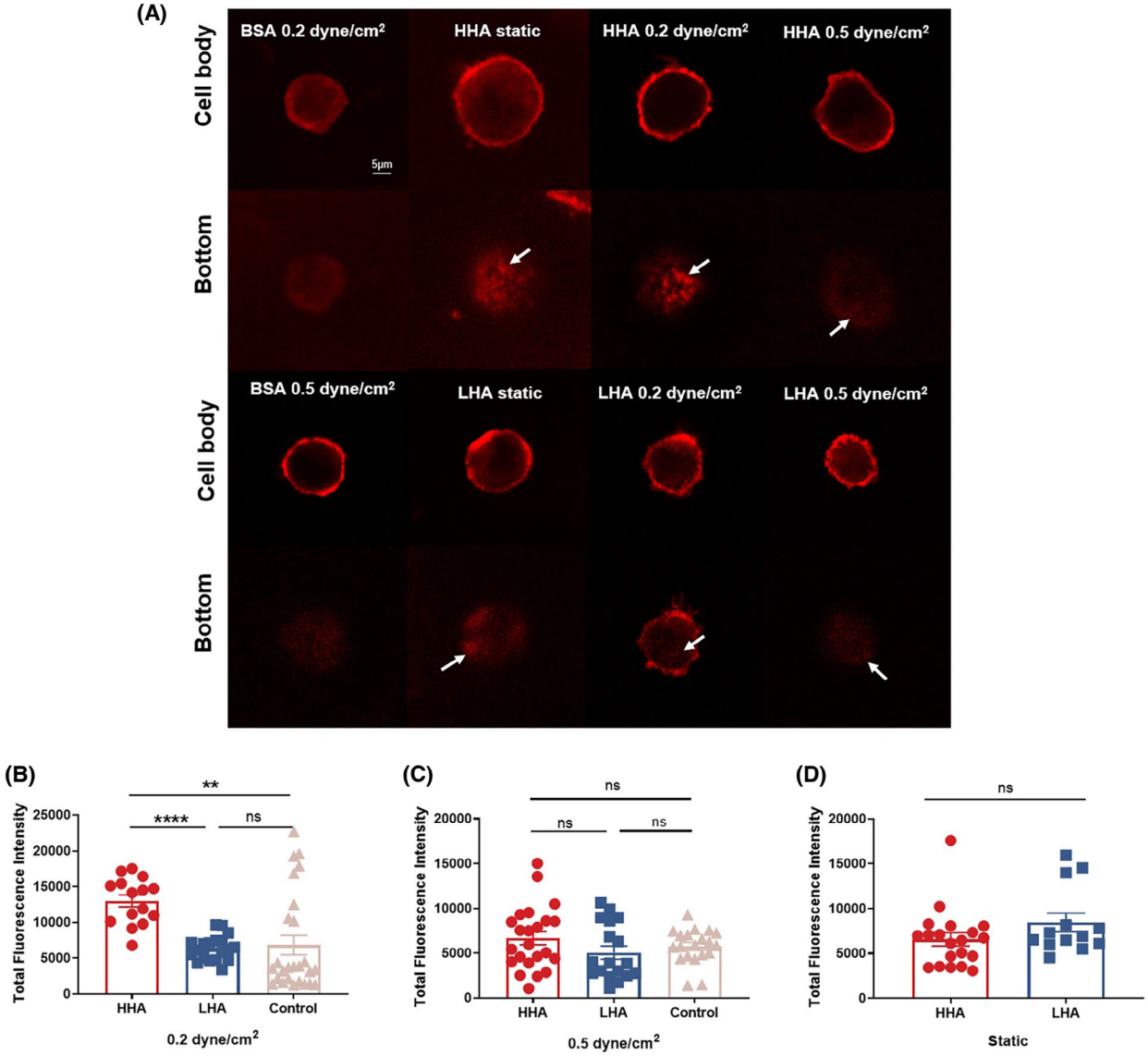

Fig. 5. Differences in CD44 expression on U937 cells induced by HHA- or LHA-CD44 interaction under static or shear flow. (A) Immunofluorescence staining of CD44 expression on adhered U937 cells after 5 min of shear flow or just static settlement with presentations focusing on both cell body and bottom. (B–D) Quantified CD44 expression on adhered U937 cells after 5 min of shear flow of 0.2 dyne·cm^{-2} (B), 0.5 dyne·cm^{-2} (C) or just static adhesion (D) for the cases of HHA, LHA or BSA-coated substrates. Arrows indicate molecular clustering of CD44 at the bottom surface. Scale bar = 5 μm. $^{**}P < 0.01$, $^{****}P < 0.0001$.

anchored HA because the incubation of soluble HHA or LHA would not induce differences in expression for CD44 or CD18 (Fig. 8C,D).

Discussion

The present study aimed to elucidate the differences between HHA and LHA for binding to CD44 under shear flow, as well as their respective abilities for inducing CD44 and CD18 expression through an intracellular signal pathway, based on the biological functions of CD44–HA interactions in mediating cell adhesion and the diversity and sensitivity of HA MW in pathophysiological alterations. Here, we found that CD44–HHA and CD44–LHA interactions were dominant in the binding and shear resistance phases, respectively. CD44–HHA interactions under shear flow of 0.2 dyne·cm^{-2} could induce significant enhancements of CD44 clustering and both CD44 and CD18 expression. Our results offer a basis for further

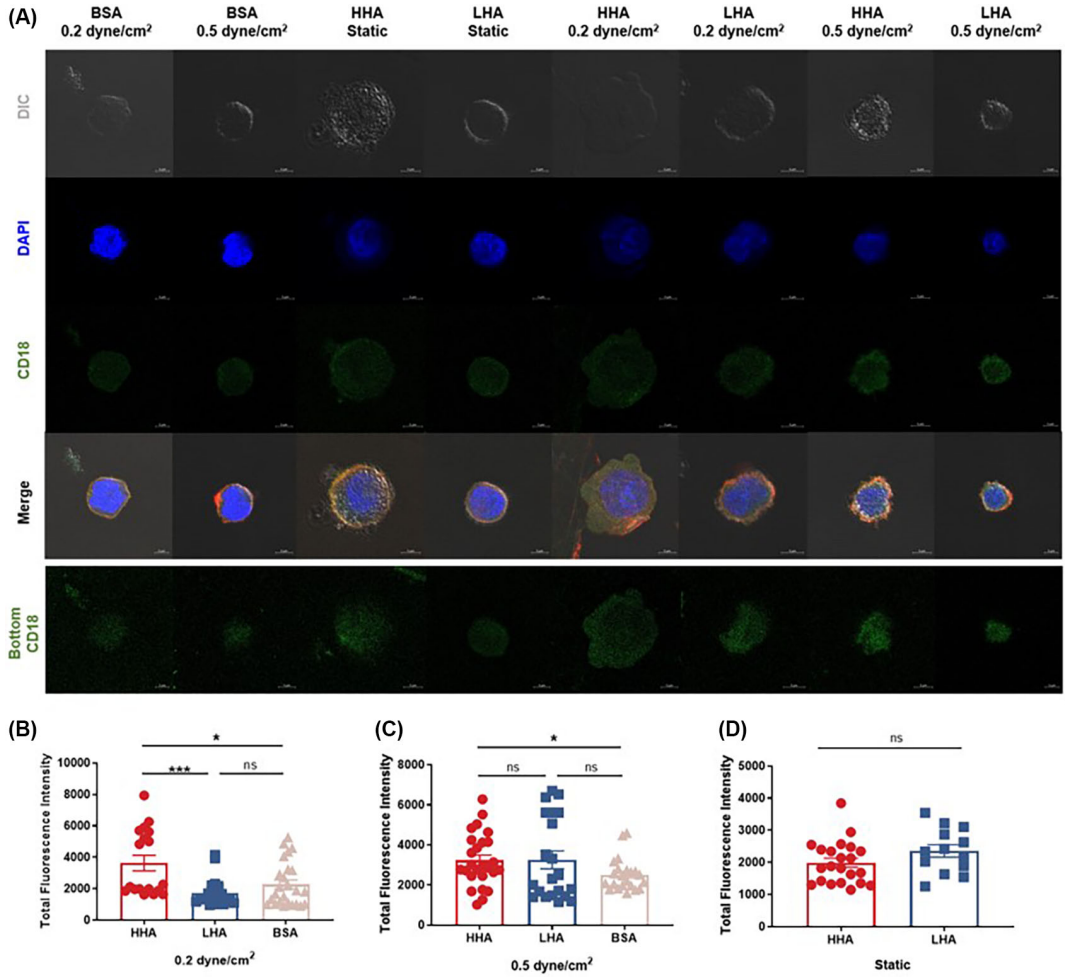

Fig. 6. Differences in CD18 expression on U937 cells induced by HHA- or LHA-CD44 interaction under static or shear flow. (A) Immunofluorescence staining of CD18 (green) on adhered U937 cells after 5 min of shear flow or static settlement. 4′,6-Diamidino-2-phenylindole (DAPI) for nuclei (blue) and differential interference contrast (DIC) are shown as the control. The bottom distribution of CD18 (bottom row) are also presented. (B–D) Quantified CD18 expression on adhered U937 cells after 5 min of shear flow of 0.2 (B), 0.5 dyne·cm^{-2} (C) or just static adhesion (D). Scale bar = 5 μm. *$P < 0.05$, ***$P < 0.001$.

understanding the biological differences between HHA and LHA in mediating cellular adhesions in inflammatory response and tumour metastasis.

External physical or mechanical factors for CD44–HA interaction are known to be critical, especially for a typical 2D receptor–ligand interaction. On the one hand, besides the presentation of a similar shear stress range of ≤ 1.0 dyne·cm^{-2} for effective CD44–HA binding as in previous studies [27,36], the present study also exhibited a threshold phenomenon between shear stresses of 0.2 and 0.5 dyne·cm^{-2}. That is, the association of CD44–HA interactions could overcome its dissociation under lower shear stresses of ≤ 0.2 dyne·cm^{-2}, resulting in a gradual increase in the adhered cell number during the binding course, whereas the association and dissociation tend to reach a balance with a constant number of adhered cells under the higher shear stresses of ≥ 0.5 dyne·cm^{-2} (Fig. 2). In addition, the effective cell accumulation that only occurred below a shear stress of 1.0 dyne·cm^{-2} indicated that CD44–HA association was not as fast as that of selectin-ligand interactions [37,38]. On the other hand, our results revealed that the disruption of CD44 clustering regulated the CD44–HA interaction and corresponding cell adhesion (Fig. 4). This is a reasonable hypothesis because the release of CD44 from local lipid raft to uniform distribution on the cell membrane would reduce the probability of an encounter between CD44 and HA and cooperation among multiple CD44–HA pairs for bond formation under shear flow, especially under conditions where both sides of CD44

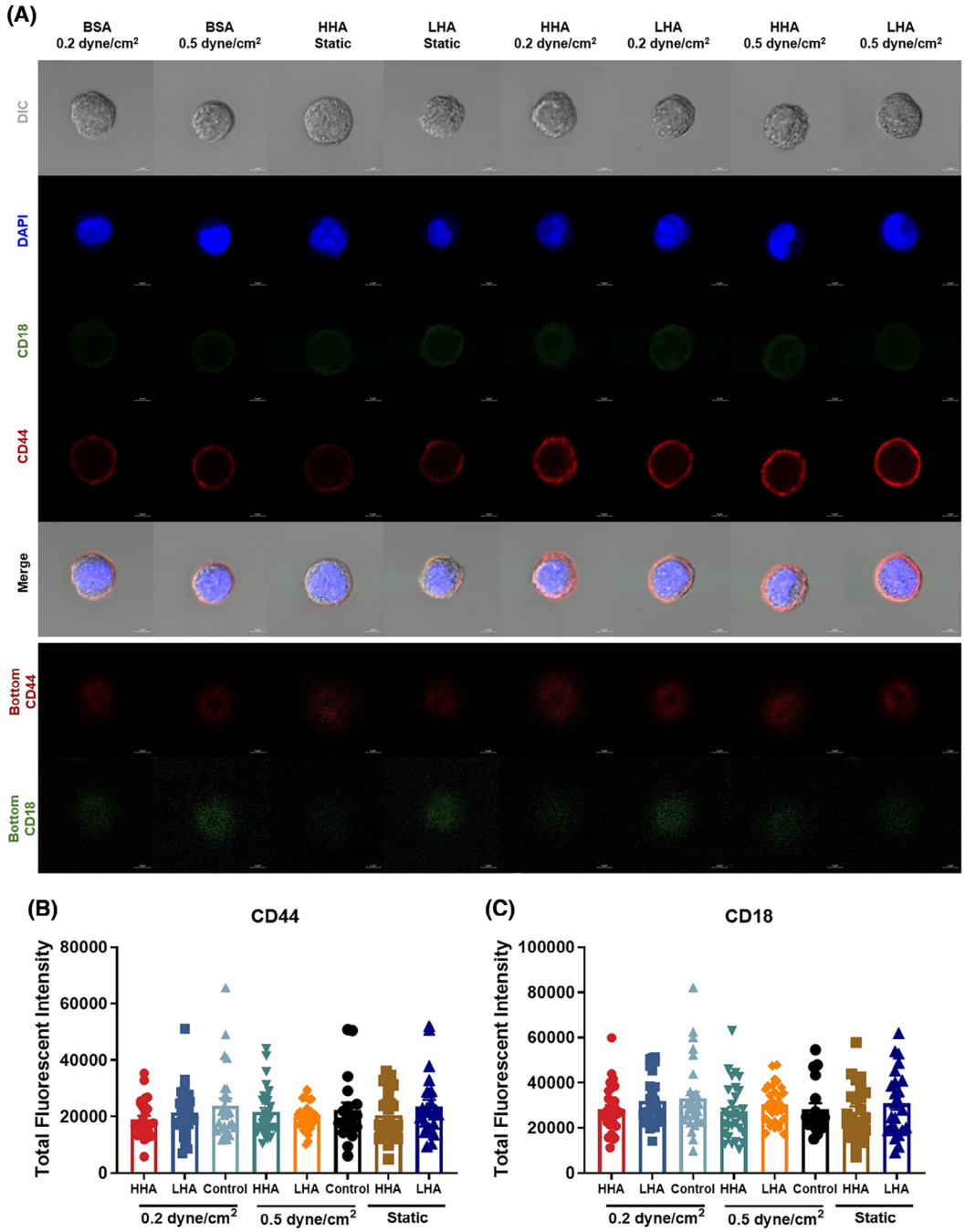

Fig. 7. Differences in CD44 and CD18 co-expression on MβCD-treated U937 cells induced by HHA- or LHA-CD44 interaction under static or shear flow. (A) Immunofluorescence staining of CD44 (red) and CD18 (green) on adhered U937 cells after 5 min of shear flow or static settlement with both presentations focusing on cell body and bottom. 4′,6-Diamidino-2-phenylindole (DAPI) for nuclei (blue) and differential interference contrast (DIC) are shown as the control. (B, C) Quantified CD44 (B) and CD18 (C) expression for all cases. Scale bar = 5 μm.

and HA were in sparse and uniform distributions [39]. However, the sparse distributions of the already formed molecular bonds are favourable for shear resistance.

The major finding from the present study are the quantifyng interaction differences between HHA and LHA to the same CD44 receptor under shear flow and

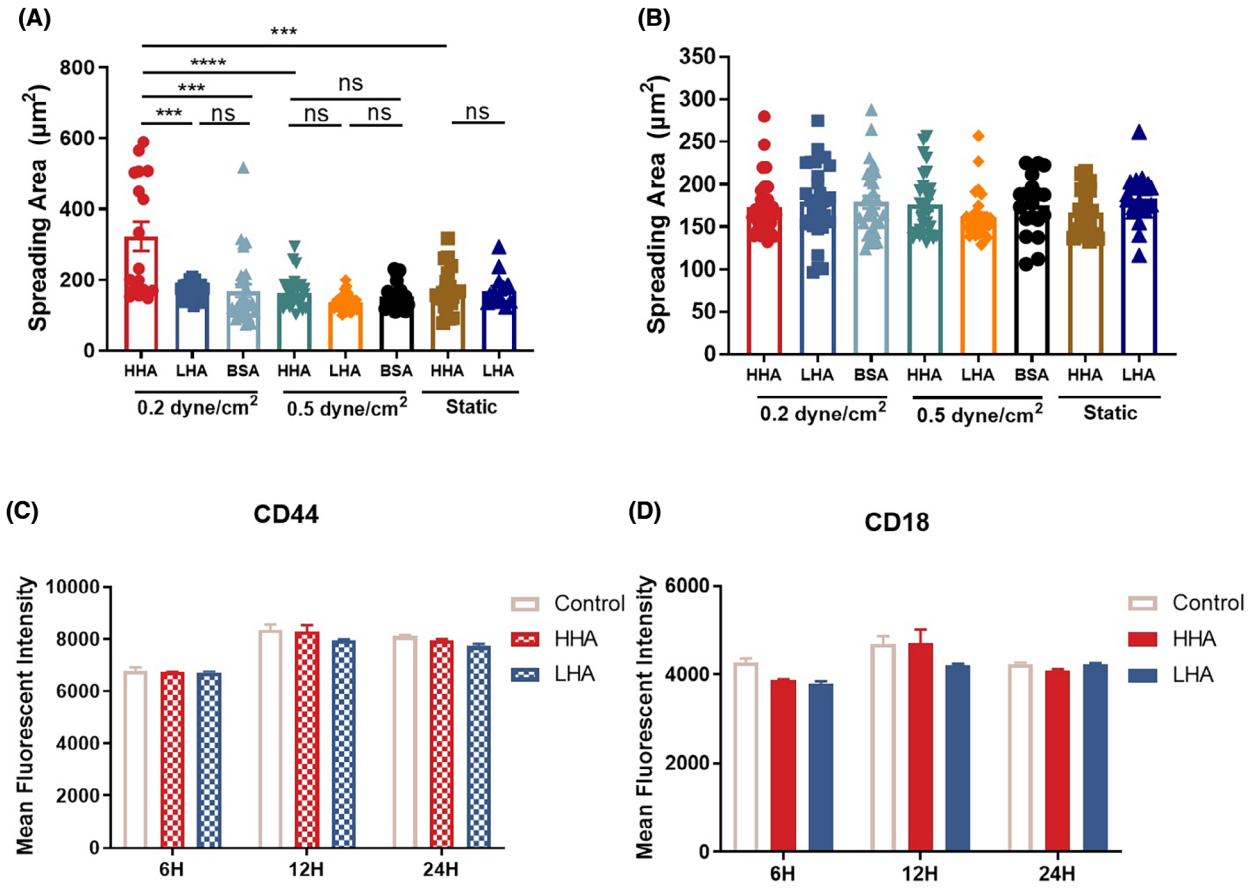

Fig. 8. Spreading area of adhered U937 cells mediated by anchored HA and their CD44 and CD18 expression induced by soluble HA incubation. (A, B) Spreading area of firmly adhered U937 cells without (A) or with (B) MβCD-treatment mediated by CD44–HHA or -LHA interactions after 5 min of shear flow or just static settlement. The case for those cells adhered to only BSA-coated substrate served as a control. (C, D) Expression of CD44 (C) and CD18 (D) on U937 cell after different soluble HHA or LHA incubation durations. The case without HA incubation was set as a control. Data are shown as the mean ± SE of at least three independent repeats. ***$P < 0.001$, ****$P < 0.0001$.

the respective abilities for inducing intracellular signals. Similar to the respectively anti- and pro-inflammatory functions of soluble HHA and LHA, surface anchored HHA and LHA respectively dominated the binding and shear resistance stage through binding to CD44. Besides the higher interaction strength of CD44–HHA interaction, we considered that the domination of HHA in the binding phase was mainly because of the large target area resulting from both CD44 clustering and HHA assembly for ready recognition and matching. Once the molecular complexes were formed, the uniform bond distribution such as CD44–LHA interaction was more favourable for shear resistance. Furthermore, CD44–HHA interaction could more effectively trigger intracellular signals than CD44–LHA interaction under shear stress of 0.2 dyne·cm^{-2}. This advantage of HHA function would disappear under the case of static conditions, a high shear stress of 0.5 dyne·cm^{-2} or disruption of the lipid raft, indicating the need for CD44 clustering and bond quantity to trigger intracellular signals. In addition, the activation of CD18 by CD44–HHA interaction also predicted the potential synergistic roles in immunological responses between CD44–HA and integrin-ligand interaction pairs, similar to the cooperation between CD44–E-selectin and LFA-1–intercellular adhesion molecule-1 interactions in a classical inflammatory cascade [33].

In summary, the present study provides basic data for elaborating the abilities of different HA MW to mediate leukocyte adhesions or recruitment by binding to CD44 under shear flow. However, the profiles of HA distributions in various tissues and the changes of HA MW under pathophysiological conditions remain

far from clear. Furthermore, the existence of both soluble and endothelial-anchored HA, especially in liver sinusoid tissue [40–43], also adds to the complexity of *in vivo* CD44–HA interactions. In addition, increased HA deposition is a common feature of inflamed tissues, such as the HA cable structure formed on activated *in vitro* cell lines [44,45] or the *in vivo* endothelial layer [10,46,47] upon various stimulations that enhances leukocyte adhesion and recruitment. Thus, competition among different HA MW and between soluble and anchored HA, as well as the distinct assembly of HA for CD44 binding and the corresponding biological functions, requires further investigation. It is well known that HA could bind to many other receptors in addition to CD44, including the hyaluronic acid receptor for endocytosis (HARE/stabilin 2) responsible for the rapid clearance of HA, the chondroitin sulfate and heparin from circulation [48], the lymph-specific LYVE-1 for mediating dendritic and other inflammatory cell egress to the lymphatic lumen [49,50], the receptor for HA-mediated motility (RHAMM/CD168) responsible for protein tyrosine phosphorylation and focal adhesion turnover [51], and the layilin for epithelial integrity [52]. Thus, the effects of HA MW on its binding ability to these receptors and their downstream signalling pathways, as well as the corresponding biological functions, also require further investigation.

Materials and methods

Reagents

Alexa Fluor® 647 anti-mouse/human CD44 Antibody (103018), Isotype Ctrl antibody of Alexa Fluor® 647 Rat IgG2b (400626), fluorescein isothiocyanate (FITC) anti-human CD18 antibody (302106) and Isotype Ctrl antibody of FITC mouse IgG1 (400108) were obtained from BioLegend (San Diego, CA, USA). Low molecular weight hyaluronan (LHA) (GLR001 ~20 kDa) and high molecular weight hyaluronan (HHA) (GLR002 ~1000 kDa) were purchased from R&D Systems (Minneapolis, MN, USA). Biotin HHA (B1557 > 700 kDa) and avidin (A9275) were purchased from Sigma-Aldrich (St Louis, MO, USA). Biotin LHA (TM2-055 20 kDa) was purchased from Greative PEGworks (Chapel Hill, NC, USA). Recombinant human CD44-his tag protein (12211-H08H) was purchased from Sino Biological Company (Beijing, China). Anti-CD44 blocking antibody Hermes-1 (MA4400) was purchased from Thermo Fisher Scientific (Waltham, MA, USA). MβCD (HY-101461) was purchased from MedChemExpress (Monmouth Junction, NJ, USA). Dulbecco's phosphate-buffered saline (DPBS) (SH30028.02) and Hank's balanced salt solution (SH30268.01) were purchased from Hyclone Company (Logan, UT, USA). Fetal bovine serum and RPMI 1640 medium (2193043) were obtained from Gibco (Grand Island, NY, USA). Penicillin–streptomycin was obtained from Thermo Fisher Scientific.

Cell culture

Human myelomonocytic leukaemia cell line U937 (NICR, Beijing, China) was prepared in RPMI 1640 medium with 10% fetal bovine serum and 1% penicillin–streptomycin. Cells were cultured at 37 °C and humidified 5% (v/v) CO_2 atmosphere with medium exchange every 24 h. Cells were collected by centrifuging at 170 ***g*** for 3 min. For cholesterol depletion, cells were washed twice with serum-free medium and then incubated with 10 mM MβCD for 15 min at 37 °C [29]. Prior to functional tests, cells were washed and resuspended at least three times using DPBS.

Flow chamber assay

The parallel-plate flow chamber assay, consisting of a flow chamber of length 2 cm × width 0.5 cm × height 0.01 inches, was assembled using a circular flow cell system (#31-001; GlycoTech, Gaithersburg, MD, USA) and was used to quantify the binding difference of CD44 to HHA or LHA. Different concentrations of HHA or LHA (2, 20, 200, 1000 $\mu g \cdot mL^{-1}$) were coated on a sterile 35-mm tissue culture dish by directly physical absorption. Briefly, 20 µL of HHA or LHA was incubated on an area of 0.5 cm × 0.5 cm for 2 h at 37 °C. Coating area was then washed three times with DPBS followed by blocking incubation of 1% BSA for 2 h, 37 °C. Flowing U937 cells were collected with a final concentration of $10^6 \cdot mL^{-1}$ after blocking incubation of 1% BSA for 2 h, 37 °C. The blocking of CD44–HHA/LHA interactions was performed by pre-incubating U937 cells with anti-CD44 blocking antibody of Hermes-1 for 30 min before the flow chamber assay [53]. Substrates without any HA coating were used as a blank control.

Each flow chamber test included two sequential phases [37]. The first one focused on testing CD44–HHA/LHA binding ability by continuously filling with U937 cells solution under a constant shear stress of 0.1, 0.2, 0.5 or 1.0 $dyne \cdot cm^{-2}$ for 300 s. The second one was performed just after the first phase by switching the U937 cells solution to blank Hank's balanced salt solution with stepwise shear stress from 1 to 48 $dyne \cdot cm^{-2}$, with 30 s of each stress, to quantify the shear-resistance of CD44–HHA/LHA interaction. The binding ability of CD44–HHA/LHA interactions was then characterized by the number of firmly adhered cells. Here, the cells were defined as firm adhesion if they kept motionless for at least 1 s. The shear-resistance of CD44–HHA/LHA interaction was defined by the

evolution of cell numbers or normalized cell numbers remaining adhered at 30 s during each stress.

Flow cytometry

Flow cytometry assay was used to quantify the constitutive expression density of CD44 or CD18 on U937 cells [37]. In brief, 5×10^4 cells were incubated with anti-CD44 or CD18 antibody at a concentration of 10 $\mu g \cdot mL^{-1}$ for 30 min on ice, then resuspended into 400 μL of DPBS. After three washes, the U937 cells were analysed using flow cytometry (BD Biosciences, San Jose, CA). Isotype Ctrl Antibody were used as a control.

AFM assay

A Bioscope MultiMode8 AFM (Bruker, Billericia, MA, USA) was used to measure the binding strength of CD44–HHA/LHA interactions [37]. Commercial MLCT cantilevers (Veeco; Bruker) were used with a nominal spring constant k_c of 10 $pN \cdot nm^{-1}$ (cantilever *C*). They were functionalized with CD44 by direct physical absorption. Briefly, the cantilevers were first incubated in 100 $\mu g \cdot mL^{-1}$ solution of CD44 for 2 h at 37 °C and then, after washing three times with DPBS, they were blocked in 1% BSA for 2 h at 37 °C. The substrates were functionalized with HHA/LHA through avidin capture. In brief, avidin (2 $mg \cdot mL^{-1}$) was physically absorbed to a fresh mica for 2 h at 37 °C, then bio-HHA/LHA (200 $\mu g \cdot mL^{-1}$) was incubated to the mica for 2 h at 37 °C. Finally, the mica was blocked with 1% BSA for 2 h at 37 °C. Substrates without any HA capture were used as a control.

HA-functionalized mica was placed on the AFM stage, which was repeatedly driven to approach the CD44-coated cantilever tip, making contact at a compressive force allowing reversible bond formation and dissociation, and retracted away to allow observation of the adhesion event and measurement of rupture force, if any. The adhesion and force signals for each approach–contact–retract cycle were collected via a quad photodetector. The approach velocity and compressive force were set as 1 $\mu m \cdot s^{-1}$ and 150 pN for all experiments, respectively. The contact time between the cantilever and mica was set as 500 ms, and five different retract velocities of 0.5, 1, 2, 4 and 8 $\mu m \cdot s^{-1}$ were set for each CD44–HHA /LHA interaction system. Each cantilever was calibrated by thermal tune method (calculated the deflection sensitivity values ranging between 180 and 200 $nm \cdot V^{-1}$) before the experiments. Different locations on each mica were tested for 100 cycles for each location. All tests were independently repeated at least three times, and each case had at least 200 adhesion events and rupture forces. Low molecular densities were used to control infrequent binding (< 35%). Besides the adhesion frequency and rupture force, the systematic spring constant *k* was also collected for demonstrating the distinct interactions of CD44–HHA/LHA.

Immunofluorescence staining and imaging

An immunofluorescence assay was used to exhibit the expression and distribution of CD44 and CD18 on U937 cells. Adhered U937 cells after 1 min of free sedimentation were then subjected to 0.2 or 0.5 $dyne \cdot cm^{-2}$ of fluid shear stress for 5 min. At the end of the stage, 4% paraformaldehyde was flowed into the chamber with gentle shear stress to fill the chamber for 15 min, follwed by washing three times. The FITC-labelled CD18 antibody (500 $\mu g \cdot mL^{-1}$, 5 μL) and 647-labelled CD44 antibody (500 $\mu g \cdot mL^{-1}$, 5 μL) were added to the samples with incubation overnight at 4 °C. After washing with PBS, Hoechst 33342 with a ratio of 1 : 1000 was added to stain nuclei for 10 min at room temperature. Stained samples were then stored at 4 °C for imaging by confocal microscopy (L710/880; Zeiss, Oberkochen, Germany). Each fluorescent cell was imaged using laminar scanning by dividing the cell into 10 layers with respect to height, with the thickness of each layer being about 1 μm. Corresponding images were analysed using IMAGEJ, version 1.53c (National Institute of Health, Bethesda, MD, USA) and the total fluorescence intensity of each cell was obtained. It should be noted that the bottom layer of each cell for imaging was about 1–2 μm above the substrate.

Statistical analysis

Student's *t*-test was performed depending on whether the data passed the normality test for two-group comparison. All statistical analyses were performed using PRISM, version 8.0 (GraphPad Software Inc., San Diego, CA, USA). All experiments were performed independently at least in triplicate and the data are presented as the mean ± SE.

Acknowledgements

This work was supported by National Natural Science Foundation of China grants (32130061, 11972042 and 12172366) and Scientific Instrument Developing Project of Chinese Academy of Sciences grant GJJSTD20220002.

Conflicts of interest

The authors declare that they have no conflicts of interest.

Author contributions

LL, ML and SL designed the research and wrote the article. LL performed the flow cytometry, flow chamber and immunofluorescence experiments. QD performed the AFM experiments. YW, ZZ, XZ and MZ analysed the data and prepared the figures.

Data availability statement

The data that support the findings of the present study are available in Figs 1–8.

References

1 Miyake K, Underhill CB, Lesley J & Kincade PW (1990) Hyaluronate can function as a cell adhesion molecule and CD44 participates in hyaluronate recognition. *J Exp Med* **172**, 69–75.

2 Lesley J, Howes N, Perschl A & Hyman R (1994) Hyaluronan binding function of CD44 is transiently activated on T cells during an in vivo immune response. *J Exp Med* **180**, 383–387.

3 DeGrendele HC, Estess P, Picker LJ & Siegelman MH (1996) CD44 and its ligand hyaluronate mediate rolling under physiologic flow: a novel lymphocyte-endothelial cell primary adhesion pathway. *J Exp Med* **183**, 1119–1130.

4 Mohamadzadeh M, DeGrendele H, Arizpe H, Estess P & Siegelman M (1998) Proinflammatory stimuli regulate endothelial hyaluronan expression and CD44/HA-dependent primary adhesion. *J Clin Invest* **101**, 97–108.

5 Siegelman MH, DeGrendele HC & Estess P (1999) Activation and interaction of CD44 and hyaluronan in immunological systems. *J Leukoc Biol* **66**, 315–321.

6 DeGrendele HC, Estess P & Siegelman MH (1997) Requirement for CD44 in activated T cell extravasation into an inflammatory site. *Science* **278**, 672–675.

7 Khan AI, Kerfoot SM, Heit B, Liu L, Andonegui G, Ruffell B, Johnson P & Kubes P (2004) Role of CD44 and hyaluronan in neutrophil recruitment. *J Immunol* **173**, 7594–7601.

8 Wolf KJ, Shukla P, Springer K, Lee S, Coombes JD, Choy CJ, Kenny SJ, Xu K & Kumar S (2020) A mode of cell adhesion and migration facilitated by CD44-dependent microtentacles. *Proc Natl Acad Sci USA* **117**, 11432–11443.

9 Krolikoski M, Monslow J & Pure E (2019) The CD44-HA axis and inflammation in atherosclerosis: a temporal perspective. *Matrix Biol* **78-79**, 201–218.

10 McDonald B, McAvoy EF, Lam F, Gill V, de la Motte C, Savani RC & Kubes P (2008) Interaction of CD44 and hyaluronan is the dominant mechanism for neutrophil sequestration in inflamed liver sinusoids. *J Exp Med* **205**, 915–927.

11 Kolaczkowska E & Kubes P (2013) Neutrophil recruitment and function in health and inflammation. *Nat Rev Immunol* **13**, 159–175.

12 Wong J, Johnston B, Lee SS, Bullard DC, Smith CW, Beaudet AL & Kubes P (1997) A minimal role for selectins in the recruitment of leukocytes into the inflamed liver microvasculature. *J Clin Invest* **99**, 2782–2790.

13 Essani NA, Fisher MA, Simmons CA, Hoover JL, Farhood A & Jaeschke H (1998) Increased P-selectin gene expression in the liver vasculature and its role in the pathophysiology of neutrophil-induced liver injury in murine endotoxin shock. *J Leukoc Biol* **63**, 288–296.

14 Fox-Robichaud A & Kubes P (2000) Molecular mechanisms of tumor necrosis factor alpha-stimulated leukocyte recruitment into the murine hepatic circulation. *Hepatology* **31**, 1123–1127.

15 Monslow J, Govindaraju P & Pure E (2015) Hyaluronan – a functional and structural sweet spot in the tissue microenvironment. *Front Immunol* **6**, 231.

16 Petrey AC & de la Motte CA (2014) Hyaluronan, a crucial regulator of inflammation. *Front Immunol* **5**, 101.

17 Cyphert JM, Trempus CS & Garantziotis S (2015) Size matters: molecular weight specificity of hyaluronan effects in cell biology. *Int J Cell Biol* **2015**, 563818.

18 Garantziotis S & Savani RC (2019) Hyaluronan biology: a complex balancing act of structure, function, location and context. *Matrix Biol* **78–79**, 1–10.

19 McKee CM, Penno MB, Cowman M, Burdick MD, Strieter RM, Bao C & Noble PW (1996) Hyaluronan (HA) fragments induce chemokine gene expression in alveolar macrophages. The role of HA size and CD44. *J Clin Invest* **98**, 2403–2413.

20 Tavianatou AG, Caon I, Franchi M, Piperigkou Z, Galesso D & Karamanos NK (2019) Hyaluronan: molecular size-dependent signaling and biological functions in inflammation and cancer. *FEBS J* **286**, 2883–2908.

21 Jiang L, Liu G, Liu H, Han J, Liu Z & Ma H (2018) Molecular weight impact on the mechanical forces between hyaluronan and its receptor. *Carbohydr Polym* **197**, 326–336.

22 Sapudom J, Ullm F, Martin S, Kalbitzer L, Naab J, Moller S, Schnabelrauch M, Anderegg U, Schmidt S & Pompe T (2017) Molecular weight specific impact of soluble and immobilized hyaluronan on CD44 expressing melanoma cells in 3D collagen matrices. *Acta Biomater* **50**, 259–270.

23 Amorim S, da Costa DS, Freitas D, Reis CA, Reis RL, Pashkuleva I & Pires RA (2018) Molecular weight of surface immobilized hyaluronic acid influences CD44-mediated binding of gastric cancer cells. *Sci Rep* **8**, 16058.

24 Mizrahy S, Raz SR, Hasgaard M, Liu H, Soffer-Tsur N, Cohen K, Dvash R, Landsman-Milo D, Bremer MG, Moghimi SM *et al.* (2011) Hyaluronan-coated nanoparticles: the influence of the molecular weight on CD44-hyaluronan interactions and on the immune response. *J Control Release* **156**, 231–238.

25 Long M, Lü SQ & Sun GY (2006) Kinetics of receptor-ligand interactions in immune responses. *Cell Mol Immunol* **3**, 79–86.

26 Li N, Lü SQ, Zhang Y & Long M (2015) Mechanokinetics of receptor-ligand interactions in cell adhesion. *Acta Mech Sin* **31**, 248–258.

27 Christophis C, Taubert I, Meseck GR, Schubert M, Grunze M, Ho AD & Rosenhahn A (2011) Shear stress regulates adhesion and rolling of $CD44^+$ leukemic and hematopoietic progenitor cells on hyaluronan. *Biophys J* **101**, 585–593.

28 Hanke M, Hoffmann I, Christophis C, Schubert M, Hoang VT, Zepeda-Moreno A, Baran N, Eckstein V, Wuchter P, Rosenhahn A *et al.* (2014) Differences between healthy hematopoietic progenitors and leukemia cells with respect to CD44 mediated rolling versus adherence behavior on hyaluronic acid coated surfaces. *Biomaterials* **35**, 1411–1419.

29 Murai T, Sato C, Sato M, Nishiyama H, Suga M, Mio K & Kawashima H (2013) Membrane cholesterol modulates the hyaluronan-binding ability of CD44 in T lymphocytes and controls rolling under shear flow. *J Cell Sci* **126**, 3284–3294.

30 Yang Z, Qin W, Chen Y, Yuan B, Song X, Wang B, Shen F, Fu J & Wang H (2018) Cholesterol inhibits hepatocellular carcinoma invasion and metastasis by promoting CD44 localization in lipid rafts. *Cancer Lett* **429**, 66–77.

31 Yang C, Cao M, Liu H, He Y, Xu J, Du Y, Liu Y, Wang W, Cui L, Hu J *et al.* (2012) The high and low molecular weight forms of hyaluronan have distinct effects on CD44 clustering. *J Biol Chem* **287**, 43094–43107.

32 Mylvaganam S, Plumb J, Yusuf B, Li R, Lu CY, Robinson LA, Freeman SA & Grinstein S (2022) The spectrin cytoskeleton integrates endothelial mechanoresponses. *Nat Cell Biol* **24**, 1226–1238.

33 Yago T, Shao B, Miner JJ, Yao L, Klopocki AG, Maeda K, Coggeshall KM & McEver RP (2010) E-selectin engages PSGL-1 and CD44 through a common signaling pathway to induce integrin alphaLbeta2-mediated slow leukocyte rolling. *Blood* **116**, 485–494.

34 Gutjahr JC, Bayer E, Yu X, Laufer JM, Hopner JP, Tesanovic S, Harzschel A, Auer G, Riess T, Salmhofer A *et al.* (2021) CD44 engagement enhances acute myeloid leukemia cell adhesion to the bone marrow microenvironment by increasing VLA-4 avidity. *Haematologica* **106**, 2102–2113.

35 Fujisaki T, Tanaka Y, Fujii K, Mine S, Saito K, Yamada S, Yamashita U, Irimura T & Eto S (1999) CD44 stimulation induces integrin-mediated adhesion of colon cancer cell lines to endothelial cells by up-regulation of integrins and c-met and activation of integrins. *Cancer Res* **59**, 4427–4434.

36 Clark RA, Alon R & Springer TA (1996) CD44 and hyaluronan-dependent rolling interactions of lymphocytes on tonsillar stroma. *J Cell Biol* **134**, 1075–1087.

37 Li L, Ding Q, Zhou J, Wu Y, Zhang M, Guo X, Long M & Lü SQ (2022) Distinct binding kinetics of E-, P- and L-selectins to CD44. *FEBS J* **289**, 2877–2894.

38 Lou J, Yago T, Klopocki AG, Mehta P, Chen W, Zarnitsyna VI, Bovin NV, Zhu C & McEver RP (2006) Flow-enhanced adhesion regulated by a selectin interdomain hinge. *J Cell Biol* **174**, 1107–1117.

39 Li L, Ji J, Song F & Hu J (2022) Intercellular receptor-ligand binding: effect of protein-membrane interaction. *J Mol Biol* **435**, 167787.

40 Fraser JR, Alcorn D, Laurent TC, Robinson AD & Ryan GB (1985) Uptake of circulating hyaluronic acid by the rat liver. Cellular localization in situ. *Cell Tissue Res* **242**, 505–510.

41 Deaciuc IV, Bagby GJ, Lang CH & Spitzer JJ (1993) Hyaluronic acid uptake by the isolated, perfused rat liver: an index of hepatic sinusoidal endothelial cell function. *Hepatology* **17**, 266–272.

42 Nobili V, Alisi A, Torre G, De Vito R, Pietrobattista A, Morino G, De Ville De Goyet J, Bedogni G & Pinzani M (2010) Hyaluronic acid predicts hepatic fibrosis in children with nonalcoholic fatty liver disease. *Transl Res* **156**, 229–234.

43 Hartley JL, Brown RM, Tybulewicz A, Hayes P, Wilson DC, Gillett P & McKiernan P (2006) Hyaluronic acid predicts hepatic fibrosis in children with hepatic disease. *J Pediatr Gastroenterol Nutr* **43**, 217–221.

44 Kota DJ, DiCarlo B, Hetz RA, Smith P, Cox CS Jr & Olson SD (2014) Differential MSC activation leads to distinct mononuclear leukocyte binding mechanisms. *Sci Rep* **4**, 4565.

45 Kaul R, Saha P, Saradhi M, Prasad RL, Chatterjee S, Ghosh I, Tyagi RK & Datta K (2012) Overexpression of hyaluronan-binding protein 1 (HABP1/p32/gC1qR) in HepG2 cells leads to increased hyaluronan synthesis and cell proliferation by up-regulation of cyclin D1 in AKT-dependent pathway. *J Biol Chem* **287**, 19750–19764.

46 Lauer ME, Aytekin M, Comhair SA, Loftis J, Tian L, Farver CF, Hascall VC & Dweik RA (2014) Modification of hyaluronan by heavy chains of inter-alpha-inhibitor in idiopathic pulmonary arterial hypertension. *J Biol Chem* **289**, 6791–6798.

47 Kessler S, Rho H, West G, Fiocchi C, Drazba J & de la Motte C (2008) Hyaluronan (HA) deposition precedes and promotes leukocyte recruitment in intestinal inflammation. *Clin Transl Sci* **1**, 57–61.

48 Harris EN, Kyosseva SV, Weigel JA & Weigel PH (2007) Expression, processing, and glycosaminoglycan binding activity of the recombinant human 315-kDa hyaluronic acid receptor for endocytosis (HARE). *J Biol Chem* **282**, 2785–2797.

49 Banerji S, Ni J, Wang SX, Clasper S, Su J, Tammi R, Jones M & Jackson DG (1999) LYVE-1, a new

homologue of the CD44 glycoprotein, is a lymph-specific receptor for hyaluronan. *J Cell Biol* **144**, 789–801.

50 Johnson LA, Banerji S, Lawrance W, Gileadi U, Prota G, Holder KA, Roshorm YM, Hanke T, Cerundolo V, Gale NW *et al.* (2017) Dendritic cells enter lymph vessels by hyaluronan-mediated docking to the endothelial receptor LYVE-1. *Nat Immunol* **18**, 762–770.

51 Hall CL, Wang C, Lange LA & Turley EA (1994) Hyaluronan and the hyaluronan receptor RHAMM promote focal adhesion turnover and transient tyrosine kinase activity. *J Cell Biol* **126**, 575–588.

52 Bono P, Rubin K, Higgins JM & Hynes RO (2001) Layilin, a novel integral membrane protein, is a hyaluronan receptor. *Mol Biol Cell* **12**, 891–900.

53 Goebeler M, Kaufmann D, Brocker EB & Klein CE (1996) Migration of highly aggressive melanoma cells on hyaluronic acid is associated with functional changes, increased turnover and shedding of CD44 receptors. *J Cell Sci* **109**, 1957–1964.